Materials Advances

ROYAL SOCIETY OF CHEMISTRY

PAPER

View Article Online
View Journal | View Issue

Cite this: *Mater. Adv.*, 2023, 4, 1326

Synergistic control of engineered nanostructures toward sensitivity and reliability of a flexible piezoresistive pressure sensor

Taehoon Hwang,†[ab] Jungyoon Seo,†[ab] Eun Ko,[a] Chanwoo Yang *[c] and Hwa Sung Lee *[ab]

Received 18th October 2022,
Accepted 18th January 2023

DOI: 10.1039/d2ma00987k

rsc.li/materials-advances

Flexible pressure sensors are among the most important flexible electronics used in various electronic skin applications, including artificial intelligence, human–machine interfaces, health monitoring, and soft robotics. To obtain piezoresistive pressure sensors with improved sensitivity and reliability in sensing performance, we investigated the correlation between the pressure-sensing performance of the sensors and the nanostructures of the sensing media with controlled nanopatterned templates. To compare the effects of nanostructures on the pressure sensor performances, two nanorod-patterned sensing media with different nanoscales were used: one was a finely nanopatterned sensing medium, while the other was a relatively large nanopatterned medium using different anodized aluminum oxide (AAO) templates, named shAAO and bhAAO, respectively. The piezoresistive pressure sensor using the shAAO-replicated sensing medium exhibited better sensitivity, faster response/recovery rate, and better sensing reliability than the bhAAO-pressure sensor. This result suggests that optimizing the nanopatterned structures should be considered in terms of the interdigitated contact that proceeds between the two electrodes to obtain high-performance pressure sensors when designing nanopatterned sensing media applied through face-to-face assembly of the nanostructured substrate.

Introduction

Flexible pressure sensors are among the most important flexible electronics for electronic skin (e-skin) applications. They can follow the shape of an arbitrary curvilinear surface and generate electrical signals under pressures generated through normal human activities such as regular physiological processes and physical contact in the body. Thus, the concept of e-skin, based on a flexible pressure sensor with high sensitivity and a wide sensing range capable of detecting the external pressures generated by ordinary touch or object manipulation, has received considerable attention in various fields, including artificial intelligence, human–machine interfaces, health monitoring, and soft robotics.[1–5] The pressure sensory system, for example, hopes to give robots the ability to feel the world through touch, skillfully grasp and grip objects, and communicate or interact with humans and other robots in a friendly manner. Flexible pressure sensors have been built based on a variety of sensing mechanisms such as piezoresistivity, piezocapacitance, piezoelectricity, and triboelectricity.[6–12] Among these, piezoresistive pressure sensors show great potential for practical applications because of their simple device structure, excellent sensitivity, affordability, and ease of application in metal coatings or nanoparticles/nanowires.[13–18] Although the pressure sensor driven by the piezoresistive mechanism often lacks the reliability and stability of the sensing signal, the above-mentioned advantages offset these problems.

Elastomeric polymers, such as polydimethylsiloxane (PDMS), have been typically used as piezoresistive pressure-sensing media for flexible pressure sensors, introduced with various regular and irregular nanopatterned structures.[18–23] These nanopatterned structures are designed by casting or coating onto pre-patterned templates, including designed silicon molds, laser-engraved molds, fabrics, self-assembled nano/microparticles, or porous polymer templates. Various studies have proven that elastomeric media with nano/micropatterned structures fabricated using a precisely controlled template are effective in manufacturing high-sensitivity pressure sensors, such as pillar, pyramidal, dome, or conical structures. These results indicate that an elastomeric medium-based piezoresistive pressure sensor with such nanostructures exhibits superior

[a] *Department of Materials Science and Chemical Engineering, Hanyang University, Ansan, 15588, Republic of Korea. E-mail: hslee78@hanyang.ac.kr*
[b] *BK21 FOUR ERICA-ACE Center, Hanyang University, 55 Hanyangdaehak-ro, Sangnok-gu, Ansan, 15588, Republic of Korea*
[c] *Advanced Nano-Surface & Wearable Electronics Research Laboratory, Heat and Surface Technology R&D Department, Korea Institute of Industrial Technology, Incheon, 21999, Korea. E-mail: chanu@kitech.re.kr*
† T. H. and J. S. contributed equally to this study.

sensing performance owing to its higher sensitivity to pressure than a planar medium-based sensor.[24–26] When considered as an extension of these studies, however, we believe that the complementary results on changes in pressure-sensing performance according to the finely controlled nanostructures are somewhat lacking.

Piezoelectric pressure sensors with regular nanopattern structures improve their sensitivity and detection range of loading pressure owing to the increased deformation sensitivity of the sensing medium to external force. In particular, piezoresistive sensors with an interdigitated nanostructured medium, that is, face-to-face assemblies of nanostructured substrates, can induce much greater changes in the contact area and localized stress concentration than those using a single nanostructured medium, resulting from the formation of extra current paths through the unsimultaneous contact of regular nanopatterns.[27–30] The geometrical morphologies of the nanopatterned media have a close relationship with the contact behavior under local pressure for the sensing performance associated with piezoresistive performance. For example, a pressure sensor with a very small nano/microstructure has high sensitivity in a low-pressure range; however, the reliability of its signal detection is lowered. In contrast, a pressure sensor with a relatively large size microstructure has excellent detection and sensing reliability; however, its sensitivity is often lower in the low-pressure range.[31–35] Therefore, the design and optimization of flexible pressure sensors or sensing medium nano/microstructures with high sensitivity and reliability in both low- and high-pressure ranges is one of the challenges that must be overcome for the practical applications of pressure sensors and electronic skins.

To investigate the correlation between the sensitivity or signal reliability of the pressure-sensing performance and the nano/microstructure of the sensing medium in flexible piezoelectric pressure sensors, we introduced nano/microstructures into an elastomeric sensing medium using an anodized aluminum oxide (AAO) template. Although PDMS is biocompatible and deformable, its application is limited to wearable e-skin devices that require extreme deformability because of their tearing properties beyond the limit of deformation. Polyurethane acrylate (PUA) is a representative elastomeric polymer with superior mechanical strength and deformation stability compared to PMDS[36–39] and was used as an elastomeric sensing medium in this study. In addition, to understand the effect of nanostructures more systematically on the pressure-sensing performance, two kinds of nanostructured PUA sensing media were prepared using AAO templates with hole diameters of 438.2 ± 12.8 nm and 291.5 ± 30.3 nm, which were named big-hole AAO (bhAAO) and small-hole AAO (shAAO), respectively. Along with the nanostructured diameters of the pressure-sensing medium, height is also one of the main factors affecting the sensing performance of the pressure sensor. Thus, the hole depth in the AAO template was set to 550 ± 50 nm to simplify the variables that affect the sensing performance. Although our results demonstrate adequate performance of pressure sensors, they can still provide essential basic information for the development of high-sensitivity pressure sensors in the future by analyzing the influence of the nanostructures of the sensing medium on the sensor performance.

Experimental section

Preparation of the AAO nanotemplates

The AAO templates were prepared by performing electropolishing and two-step anodization of pure aluminum sheets (99.999%, Goodfellow). The specimens were electropolished in a mixture of perchloric acid and ethanol (1 : 4 volume ratio of $HClO_4 : C_2H_5OH$) at 7 °C for 5 min at a fixed voltage of 20 V to remove surface irregularities. Anodization was then performed with 0.1 M phosphoric acid (85%, Aldrich) at 0 °C for 16 h at a voltage of 195 V. Following first anodization, the porous alumina layer was etched away with an alumina etchant (1.8 wt% chromic acid and 6 wt% phosphoric acid at 65 °C for 2 h), and the second anodization was performed under conditions identical to those of the first. The anodizing time was used to control the pore length. After the second anodization, the pores in each AAO template were widened by immersing the specimen in a 0.1 M phosphoric acid solution at 30 °C. The widening time was used to control the pore diameter.

Surface modification of AAO nanotemplates

Prior to fabrication of AAO-replicated polyurethane acrylate (PUA, Minuta Tech.) sensing medium, the AAO nanotemplate was modified with octadecyltrichlorosilane (ODTS) to facilitate the peel-off process of the elastomeric PUA film. First, the AAO nanotemplates were treated with an ozone generator for 10 min to clean the AAO surfaces before the deposition of the ODTS layers. The ODTS material was purchased from Sigma-Aldrich and was used as received. After injecting 20 mL of anhydrous toluene into the prepared vacuum-dried reaction flask, argon gas (99.97%) was added, the cleaned AAO nanotemplates were put in, and the ODTS was added to the flask (10 mM). The flask was left for 3 h under argon gas to self-assemble and modify the nanotemplate surface. The resulting nanotemplate was removed from the flask, rinsed several times with toluene, and heated in an oven at 120 °C for 20 min. Subsequently, the nanotemplate was cleaned by ultrasonication in toluene, rinsed several times with toluene and ethanol, and dried under vacuum.

Fabrication of AAO-replicated PUA sensing medium and pressure sensor

To allow PUA to penetrate the ODTS-modified AAO nanotemplate well, PUA was poured twice through a syringe onto the template surface. After pouring 0.3 mL of PUA first, it was stored in a vacuum for 1 h, waiting for the PUA to fill the nanopores. Then, additional PUA was poured to adjust the thickness of the sensing medium which was set to 0.7 mm. Subsequently, the PUA was cured by UV irradiation for 1 h. After the coated PUA was cured, the PUA film formed on the ODTS-modified AAO nanotemplate was carefully peeled off in the

vertical direction at a constant speed of approximately 2 mm s^{-1}. The 30 nm-thick Au was thermally deposited on a nanopatterned PUA surface peeled off from the AAO template to impart conductive properties. Finally, the two AAO-replicated PUA substrates were stacked together to complete the fabrication of the PUA sensing medium for the piezoresistive pressure sensor.

Characterization of structures and sensor performance

The morphologies of the AAO nanotemplate and replicated PUA sensing medium were characterized using a field-emission scanning electron microscope (SEM, Hitachi S-4200). The statistical distributions of the diameter, number density, and surface coverage of the PUA nanorods were analyzed using the ImageJ program. The sensing performance of the piezoresistive pressure sensor was assessed by measuring the current variations using an Agilent 4284A Precision LCR meter. The pressure or flexion sensing capabilities of the sensor were characterized using a home-built sensor probe station outfitted with a programmable *xy*- and *z*-axis moving stage with a 50 nm resolution and a force gauge (Mark-10, Electromatic Equip't Co., Inc.), all interfaced through a computer. The force gauge measured the applied load and the corresponding pressure was calculated by dividing the probe with the area.

Results and discussion

Fig. 1(a) schematically illustrates the fabrication steps for a flexible piezoresistive pressure sensor using a well-nanopatterned AAO template with a closely packed regular array of hexagonal columnar cells with parallel pores. To facilitate the peel-off process of elastomeric PUA films, we first introduced ODTS to the AAO template surface to reduce the adhesion energy between PUA and AAO surfaces.[40,41] After pouring PUA on the AAO template surface, it was stored in a vacuum for 1 h, waiting for the PUA to fill the nanopores. After the coated PUA was cured using UV irradiation and peeled off, a nanostructured PUA substrate was obtained. To impart piezoresistive properties, Au was deposited on a nanopatterned PUA substrate with a thickness of 30 nm, and then the two substrates were stacked together to complete the fabrication of the PUA sensing medium. Fig. 1(b) schematically illustrates the principle that the current level (or resistance) changes as the contact area increases with the deformation of the fabricated PUA sensing medium by external pressure. As aforementioned, we used AAO templates with two different pore sizes to determine the effect of the nanostructure of the sensing medium on the pressure-sensing signal. Fig. 1(c) shows the SEM images of the top- and cross-sectional views of the AAO templates having pore sizes of 438.2 ± 12.8 nm (bhAAO) and 291.5 ± 17.3 nm (shAAO) with approximate pore depths of 686.7 ± 18.2 nm and 647.7 ± 16.3 nm, respectively. The slight difference in the pore depths is owing to the anodizing process conditions for fabricating the AAO templates, which is negligible within the error range of only 5.7%. Fig. 1(d) shows the SEM images of the nanopatterned PUA substrates onto which the AAO templates were transferred, which confirmed that the pore structures of the template were well replicated as PUA sensing media.

The nanorod diameter distributions of the nanopatterned PUA substrates peeled off from the bhAAO and shAAO templates are shown in Fig. 2. The nanorod diameters of the bhAAO- and shAAO-replicated PUAs show a Gaussian

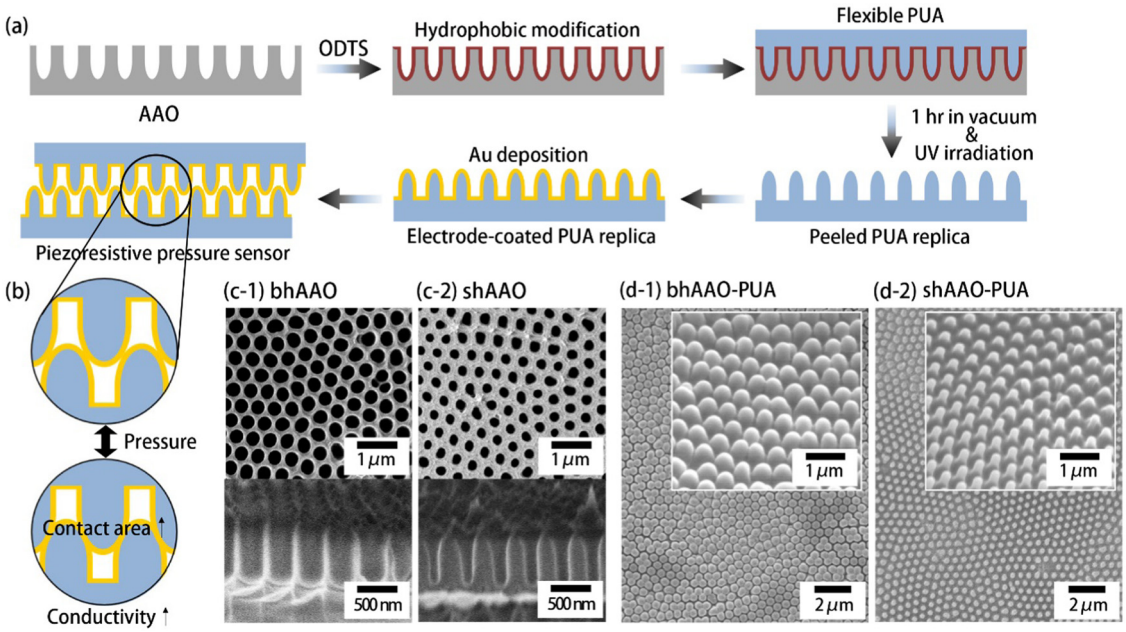

Fig. 1 Schematic illustrations of (a) the fabrication process and (b) the nanorod-interdigitated structure for a flexible piezoresistive pressure sensor. (c) Top- and cross-sectional SEM images of (c-1) bhAAO and (c-2) shAAO templates. (d) SEM images of top- and side-views of nanopatterned rod structures for the (d-1) bhAAO- and (d-1) shAAO-replicated PUA sensing media.

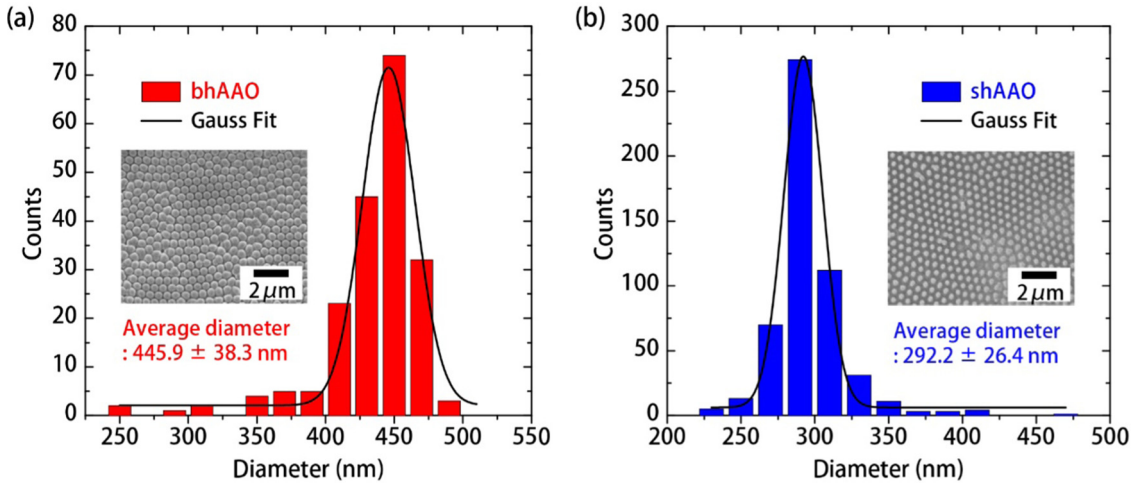

Fig. 2 The diameter distributions of (a) bhAAO- and (b) shAAO-replicated PUA nanorods. (Insets show their top-view SEM images.)

distribution and the average diameters of them are 445.9 ± 38.3 nm and 292.2 ± 26.4 nm, respectively. The average diameters of the measured nanorods were slightly larger than the pore size of the AAO templates because the penetrating PUA polymer solidifies, relieves the pressure inside the pores, and expands slightly.[42] More importantly, this is because of the uniformity of the nanopatterned

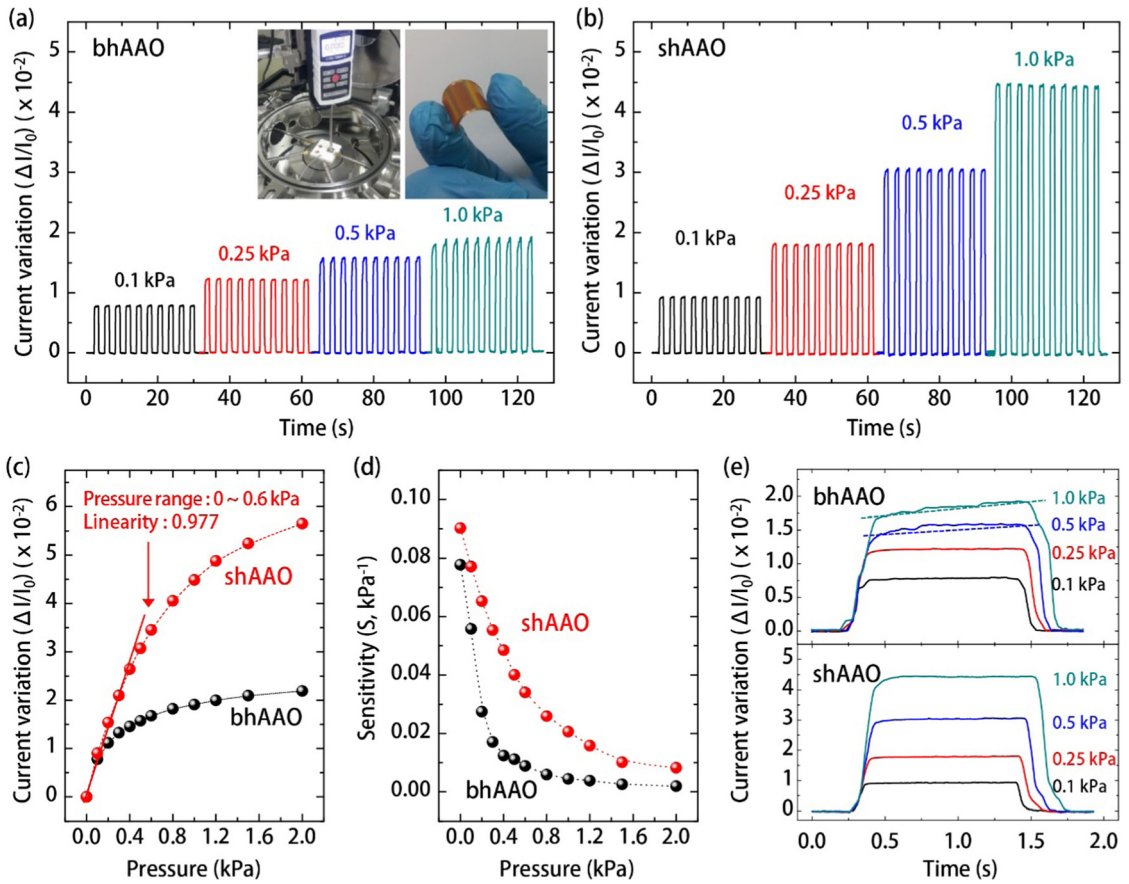

Fig. 3 Pressure-sensing performances of flexible piezoresistive pressure sensors with (a) bhAAO- and (b) shAAO-replicated PUA sensing media based on nanostructured PUA. The real-time $\Delta I/I_0$ variations were measured using repeated loading and unloading under stepwise increasing pressures of 0.1, 0.25, 0.5, and 1.0 kPa at a fixed voltage of 0.1 V. (c) The $\Delta I/I_0$ variations of bhAAO- and shAAO-pressure sensors as a function of pressure from 0 to 2.0 kPa. (d) The instantaneous sensitivity (S) variation calculated from (c) as a derivative at each pressure point for the bhAAO- and shAAO-pressure sensors. (e) Enlarged $\Delta I/I_0$ variations of the bhAAO- and shAAO-pressure sensors under constant pressures from 0.1 to 1.0 kPa. The photographs inserted in (a) show the measurement device used in the experiment and actual pressure sensor.

nanorod structures. For the bhAAO- and shAAO-replicated cases, the error ranges of the PUA nanorod diameters were confirmed as 8.6 and 9.0%, respectively, compared to their average values. This result indicates that the uniformity of the nanorod-patterned PUA with AAO templates is excellent.

Piezoresistive pressure sensors were fabricated by superimposing two nanorod-patterned PUAs coated on the surface with 30 nm-thick Au as an electrode. Fig. 3(a and b) show the pressure-sensing performance of the piezoresistive pressure sensors based on the bhAAO- and shAAO-replicated PUAs according to various pressure degrees, which were evaluated by applying a fixed voltage of 0.1 V between the two electrodes. For simplicity of nomenclature, the bhAAO- and shAAO-replicated PUA-based sensors are denoted as bhAAO- and shAAO-pressure sensors, respectively. In the absence of external pressure, the current value is low because of the small contact area between the two Au-coated nanorod-patterned PUAs. When an external pressure is applied, the PUA films are compressed together, increasing the current between the electrodes with increasing contact area. As shown in Fig. 3(a and b), the bhAAO- and shAAO-pressure sensors showed excellent repeatability when loading and unloading were repeated 10 times at pressures of 0.1, 0.25, 0.5, and 1.0 kPa, respectively. In particular, the shAAO case shows a more sensitive $\Delta I/I_0$ variation with pressure than the bhAAO case, which is summarized in Fig. 3(c). Comparing the bhAAO- and shAAO-pressure sensors, the shAAO shows a more sensitive change in $\Delta I/I_0$ values with applied pressure, and the saturation phenomenon, a chronic problem of flexible pressure sensors, is significantly improved. In addition, the shAAO-pressure sensor presented a high linearity of 0.977 in the pressure range from 0 to 0.6 kPa, which indicates that the pressure-sensing signal reliability is relatively outstanding.

The slope of the $\Delta I/I_0$ variation curve as a function of pressure is defined as the sensitivity (S), which is derived by the equation $S = (dI/I_0)/dP$, where dI is the instantaneous change in the current (I), I_0 is the initial I, and dP is the instantaneous change in the applied pressure. Fig. 3(d) shows the variations in S derived from the pressure-sensing performance of the bhAAO- and shAAO-pressure sensors. As shown,

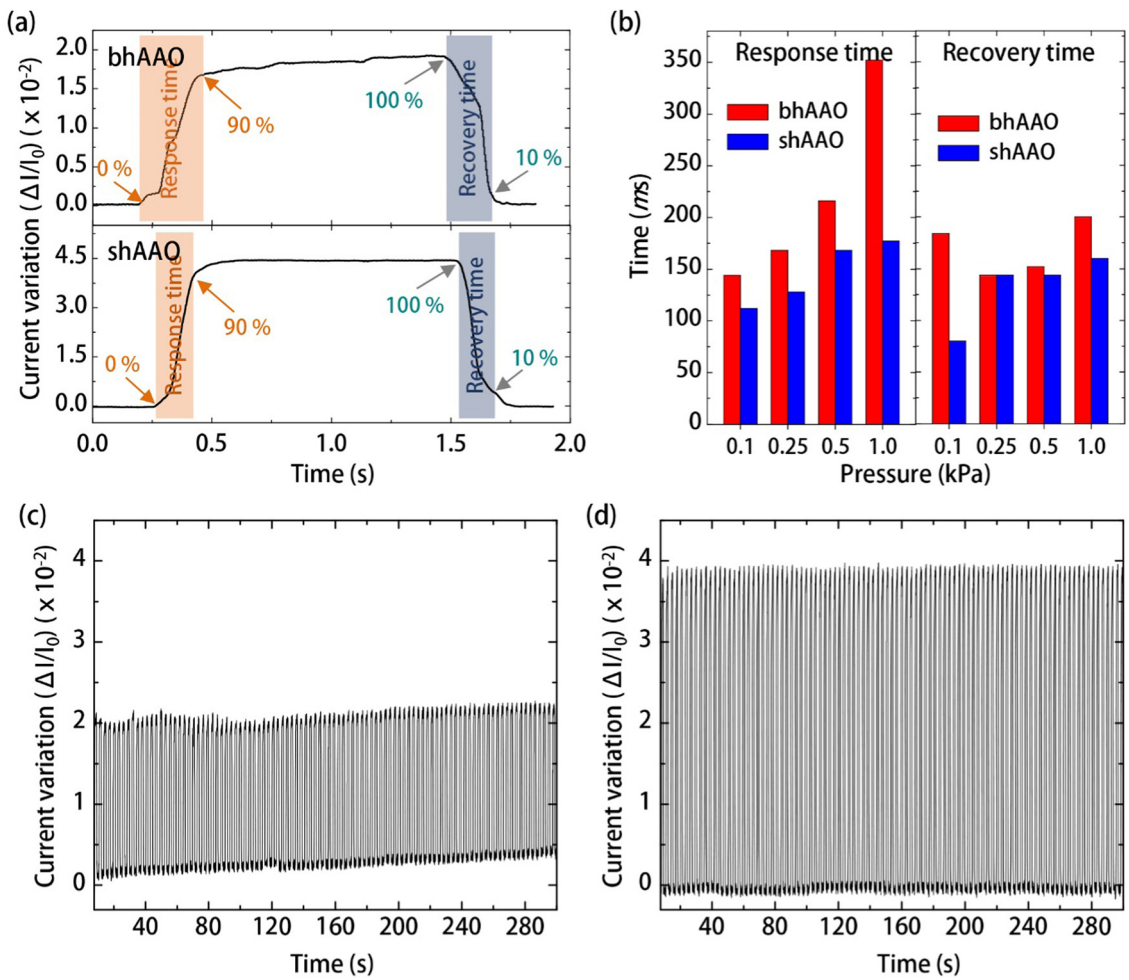

Fig. 4 (a) The explanation of the definitions used in this study to calculate the response and recovery times. These are the enlarged results of the pressure-sensing signal measured at a pressure of 1.0 kPa. (b) Summaries of response and recovery times of bhAAO- and shAAO-pressure sensors obtained at different pressures from 0.1 to 1.0 kPa. Real-time $\Delta I/I_0$ variations of (c) bhAAO- and (d) shAAO-pressure sensors under 100 loading and unloading cycles at a pressure of 0.5 kPa.

the shAAO has an overall higher S value than bhAAO, and clearly shows that the saturation problem appears later. For example, for the bhAAO-pressure sensor, the saturation of the sensing signal appears from 0.3 kPa, whereas the signal saturation for the shAAO is observed at a high applied pressure level of 1.5 kPa, despite continuous decrease in the S value. Along with the differences in the signal saturation phenomenon and the S variation, the shAAO-pressure sensor showed better performance in terms of the stability of the detected signal. As shown in Fig. 3(e), when the pressure is kept constant for a certain period of time in the range of 0.1 to 1.0 kPa, the shAAO-pressure sensor showed a constant $\Delta I/I_0$ variation at all pressures, whereas the bhAAO showed an increase in $\Delta I/I_0$ variation at relatively high pressures of 0.5 and 1.0 kPa. These results indicate that the shAAO-based piezoresistive pressure sensor with a finer nanopatterned sensing medium has a more stable response to applied pressure than the bhAAO-pressure sensor. This is a natural result because the amount and time of deformation required increases as the level of applied pressure increases.

To compare the sensing rates of the developed piezoresistive bhAAO- and shAAO-pressure sensors, the response and recovery times were analyzed. For a reliable comparison, the response time is defined as the time from the initial $\Delta I/I_0$ value without applied pressure to the point where the $\Delta I/I_0$ reached 90% level relative to the signal saturation section, while the recovery time is defined as the time to reach the point where the $\Delta I/I_0$ drops to 10% level relative to the saturated signal. These definitions are shown in Fig. 4(a), using the sensing signal when a pressure of 1.0 kPa is applied. Fig. 4(b) summarizes the results of analyzing the response and recovery times. As shown, the shAAO-pressure sensor exhibited that the time required for $\Delta I/I_0$ variations in both the processes of deformation and recovery is faster than that of the bhAAO. Moreover, a tendency for the response and recovery times to increase with the applied pressure was observed for both pressure sensors, which is consistent with the results shown in Fig. 3(e). We believe that this is a natural result because the deformation degree and time required increases as the applied pressure level increases. Fig. 4(c and d) show the real-time $\Delta I/I_0$ variation measured in loading and unloading cycles with a fixed pressure of 0.5 kPa to evaluate the long-term operational stability of the bhAAO- and shAAO-pressure sensors, respectively. For the bhAAO case, because of the relatively low sensor performance described above, the baseline in the unloaded state of pressure does not return to zero and gradually increases during 100 cycles of repeated operation, which could result in the hysteresis problem of the sensing signal. In contrast, the shAAO-pressure sensor exhibited high sensing stability without noticeable changes under the process of periodic pressure loading and unloading in cyclic operations for a long time, during which the detected $\Delta I/I_0$ fluctuation value was maintained and reproduced almost as it originally was. While previously reported piezoresistive pressure sensors[43–45] exhibited an upward or downward moving baseline like the bhAAO pressure sensor, the shAAO pressure sensor showed superior reliability with a constant baseline without hysteresis.

The morphological characteristics of the bhAAO- and shAAO-replicated PUA sensing media and the sensing performances of the piezoresistive pressure sensors are summarized in Table 1. From the information shown in the table, we can infer that the shAAO-pressure sensor performs better than the bhAAO sensor. The nanorod density of the shAAO-replicated PUA sensing medium is 4.01 μm^{-2}, which is higher than 3.84 μm^{-2} of the bhAAO case, resulting in improved current change responsiveness and pressure sensitivity at low-pressure level. A similar interpretation is supported by Kim *et al.*, who observed that the sensitivity of a piezoresistive pressure sensor is proportional to the nanostructure density.[46–48] In addition, the nanorods of the shAAO-replicated PUA exhibited a smaller diameter of 292.2 ± 26.4 nm, resulting in a low surface coverage of 34.6%. Therefore, the contact area between the upper and lower PUA nanorods can be changed sensitively because of their easy engagement with the pressure applied to the sensing medium, which improves the sensitivity and linearity of the sensing signals in the shAAO-pressure sensor. Of course, these results do not generalize that piezoresistive pressure sensors perform better when using finer-patterned sensing media at nanoscales. In designing a piezoresistive sensing medium that has superior responsiveness depending on the applied pressure, optimizing the nanopatterned structures is necessary, considering not only the nanostructure density but also the surface coverage in terms of the interdigitated contact between the two electrodes. Based on this design, it is possible to secure piezoresistive pressure sensors with improved sensitivity and reliability for sensing performance.

Fig. 5(a) shows the reproducibility test results at various applied pressures for a shAAO-pressure sensor with excellent sensitivity, reliability, and response characteristics of the sensing signal. The applied pressure was incremented from 0.25 to 2.0 kPa in 5 repetition cycles. As shown, the sensing signals of $\Delta I/I_0$ variations for the pressure sensor operated in these processes were confirmed to be constant and uniform indicating the excellent sensing performance of the developed shAAO-pressure

Table 1 Summaries of morphological characteristics of nanorod-patterned PUA sensing medium and sensing performances of piezoresistive pressure sensors

	Characteristics of nanorod-patterned PUA			Pressure-sensing performances		
	Nanorod diameter (nm)	Nanorod density (μm^{-2})	Surface coverage of nanorods (%)	Sensitivity (kPa^{-1}, at 0.2 kPa)	Response time (ms, at 1.0 kPa)	Recovery time (ms, at 1.0 kPa)
bhAAO	445.9 ± 38.3	3.84	74.3	0.0275	352.3	177.2
shAAO	292.2 ± 26.4	4.01	34.6	0.0653	199.8	159.5

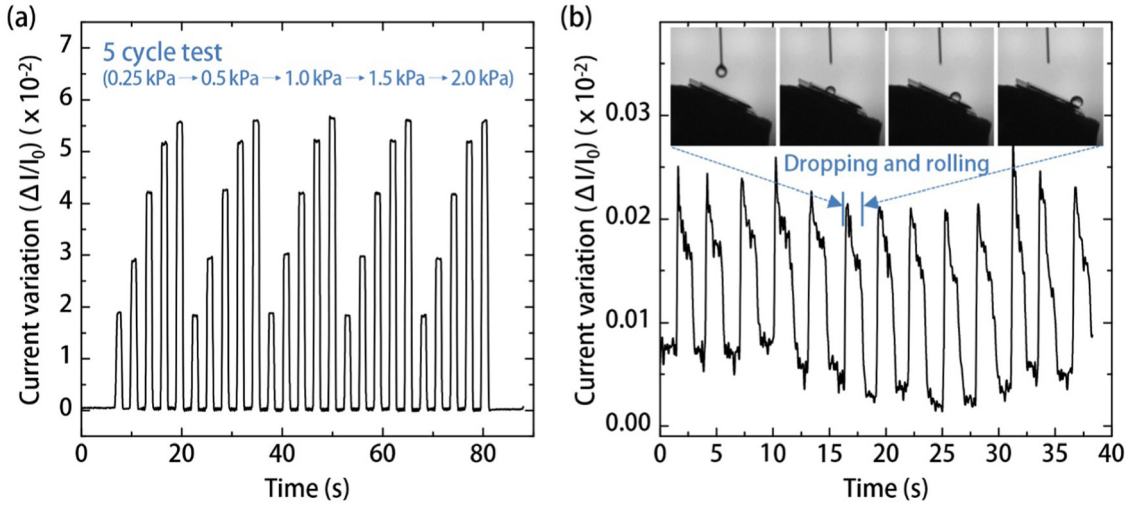

Fig. 5 (a) Five cycle reproducibility tests of the shAAO-pressure sensor in the pressure range of 0.25 to 2.0 kPa. (b) Sensing performance measured repeatedly while dropping water droplets on the tilted shAAO-pressure sensor. Inserted photographs in (b) show water droplet falling and rolling over the sensor.

sensor. All measurements of the shAAO-pressure sensor were performed at a low voltage of 0.1 V, and the initial current was ~4 mA, resulting in a static power consumption of 0.4 mW, which is comparable to those of previously reported low power piezoresistive pressure sensors.[49,50] In addition, for determining whether the shAAO-pressure sensor responds accurately to a minute pressure signal, we repeatedly measured the sensing signal by dropping small water droplets, as shown in Fig. 5(b). The process of dropping a water droplet onto the shAAO-pressure sensor in an inclined state was monitored and this process is shown in the camera-captured images in the insert of Fig. 5(b). When the droplet first falls and reaches the sensor surface, an additional force is applied by the falling speed, and thus, the sensing signal is actually detected. Subsequently, the detection signal decreases with the droplet rolling off the surface. The measured $\Delta I/I_0$ value at the midpoint of the sensing signal, which could be predicted to be the point where the drop force of the water droplet can be neglected, was 0.11×10^{-3}. Considering the weight (4.2 mg) of the water droplet measured on a sophisticated scale and the area of the electrode, the calculated pressure was 1.45 Pa, which was confirmed to be almost consistent with the measured $\Delta I/I_0$ value. These results prove that the developed shAAO-pressure sensor exhibited excellent performance that can sensitively detect even minute pressure changes.

Conclusions

In summary, we investigated the correlation between the sensitivity or signal reliability of the pressure-sensing performance and nanostructures of the sensing medium in flexible piezoelectric pressure sensors with controlled nanorod structures using AAO templates. To compare the effects of nanostructures on the pressure sensor performance, two nanorod-patterned PUA sensing media with different diameters were applied: bhAAO- (445.9 ± 38.3 nm) and shAAO-replicated (292.2 ± 26.4 nm). In addition, the shAAO-replicated sensing medium had a relatively higher density and lower surface coverage of nanorod-patterned structures. It was confirmed that the pressure sensor using the shAAO-replicated sensing medium exhibited better sensitivity, faster response/recovery rate, and better sensing reliability than the bhAAO-pressure sensor. Although the results demonstrated in this study cannot be generalized, piezoresistive pressure sensors performed better when using finer-patterned sensing media at the nanoscale. Optimizing the nanopatterned structures should be considered in terms of the interdigitated contact proceeding between the two electrodes to obtain high-performance piezoresistive pressure sensors, having a superior responsiveness depending on the applied pressure, when designing the nanopatterned sensing media with the face-to-face assembled structures of the nanostructured substrate. Our results provide essential information for the development of highly sensitive and reliable piezoresistive pressure sensors in the future.

Author contributions

Taehoon Hwang – data curation, formal analysis, and writing (original draft). Jungyoon Seo – formal analysis and data curation. Eun Ko – formal analysis. Chanwoo Yang – methodology, data curation, validation, writing (original draft), and writing (review & editing). Hwa Sung Lee – conceptualization, funding acquisition, supervision, writing (original draft), and writing (review & editing)

Conflicts of interest

The authors declare no conflicts of interest.

Acknowledgements

This work was supported by the Korea Institute for Advancement of Technology (KIAT) grant funded by the Korean Government (MOTIE) (P0008425, The Competency Development Program for

Industry Specialist), the framework of international cooperation program managed by the National Research Foundation of Korea (2021K1A3A1A20003483), and the Industry-leading Core Production Technology Development Project of the Korea Institute of Industrial Technology (KITECH, EO220006) from the Ministry of Economy and Finance, Republic of Korea.

References

1 L. Li, J. Zheng, J. Chen, Z. Luo, Y. Su, W. Tang, X. Gao, Y. Li, C. Cao, Q. Liu, X. Kang, L. Wang and H. Li, *Adv. Mater. Interfaces*, 2020, **7**, 2000743.
2 J. Chen, Y. Zhu, X. Chang, D. Pan, G. Song, Z. Guo and N. Naik, *Adv. Funct. Mater.*, 2021, **31**, 2104686.
3 S. Pyo, J. Lee, K. Bae, S. Sim and J. Kim, *Adv. Mater.*, 2021, **33**, 2005902.
4 J. Yang, J. Mun, S. Kwon, S. Park, Z. Bao and S. Park, *Adv. Mater.*, 2019, **31**, 1904765.
5 R. Yin, D. Wang, S. Zhao, Z. Lou and G. Shen, *Adv. Funct. Mater.*, 2021, **31**, 2008936.
6 W. Zhang, Y. Xiao, Y. Duan, N. Li, L. Wu, Y. Lou, H. Wang and Z. Peng, *ACS Appl. Mater. Interfaces*, 2020, **12**, 48938–48947.
7 Y. Lee, J. Park, S. Cho, Y. Shin, H. Lee, J. Kim, J. Myoung, S. Cho, S. Kang, C. Baig and H. Ko, *ACS Nano*, 2018, **12**, 4045–4054.
8 P. Zhu, Y. Wang, M. Sheng, Y. Wang, Y. Yu and Y. Deng, *J. Mater. Chem. A*, 2019, **7**, 8258.
9 Y. Huang, X. Fan, S. Chen and N. Zhao, *Adv. Funct. Mater.*, 2019, **29**, 1808509.
10 H. Shi, M. Al-Rubaiai, C. M. Holbrook, J. Miao, T. Pinto, C. Wang and X. Tan, *Adv. Funct. Mater.*, 2019, **29**, 1809116.
11 K. He, Y. Hou, C. Yi, N. Li, F. Sui, B. Yang, G. Gu, W. Li, Z. Wang, Y. Li, G. Tao, L. Wei, C. Yang and M. Chen, *Nano Energy*, 2020, **73**, 104743.
12 Y. Jang, J. Jo, K. Woo, S. H. Lee, S. Kwon, H. Kim and H. S. Lee, *Phys. Rev. Appl.*, 2019, **11**, 014037.
13 O. Kanoun, A. Bouhamed, R. Ramalingame, J. R. Bautista-Quijano, D. Rajendran and A. Al-Hamry, *Sensors*, 2021, **21**, 341.
14 Q. Zhou, B. Ji, Y. Wei, B. Hu, Y. Gao, Q. Xu, J. Zhou and B. Zhou, *J. Mater. Chem. A*, 2019, **7**, 27334–27346.
15 J. Yu, X. Hou, M. Cui, S. Zhang, J. He, W. Geng, J. Mu and X. Chou, *Nano Energy*, 2019, **64**, 103923.
16 Q. Zhou, B. Ji, G. Chen, Y. Ding, J. Wu, J. She, S. Wang and B. Zhou, *ACS Appl. Nano Mater.*, 2019, **2**, 7178–7187.
17 Y. Liu, H. Wang, W. Zhao, M. Zhang, H. Qin and Y. Xie, *Sensors*, 2018, **18**, 645.
18 Z. Lou, L. Wang, K. Jiang and G. Shen, *Nano Today*, 2019, **26**, 176–198.
19 S. Baek, H. Jang, S. Kim, H. Jeong, S. Han, Y. Jang, D. Kim and H. Lee, *RSC Adv.*, 2017, **7**, 39420–39426.
20 L. Wang, Z. Fei, Y. Qi, C. Zhang, L. Zhao, Z. Jiang and R. Maeda, *ACS Appl. Energy Mater.*, 2022, **5**, 7091–7114.
21 S. Kim, S. Mondal, B. Min and C. Choi, *ACS Appl. Mater. Interfaces*, 2018, **10**, 36377–36384.
22 Y. Mao, B. Ji, G. Chen, C. Hao, B. Zhou and Y. Tian, *ACS Appl. Nano Mater.*, 2019, **2**, 3196–3205.
23 Y. Lee, O. Kweon, H. Kim, J. Yoo, S. Han and J. Oh, *J. Mater. Chem. C*, 2018, **6**, 8569–8612.
24 C. Li, S. Yang, Y. Guo, H. Huang, H. Chen, X. Zuo, Z. Fan, H. Liang and L. Pan, *Chem. Eng. J.*, 2021, **426**, 130364.
25 A. Kalkal, S. Kumar, P. Kumar, R. Pradhan, M. Willander, G. Packirisamy, S. Kumar and B. D. Malhotra, *Addit. Manuf.*, 2021, **46**, 102088.
26 J. Chen, J. Liu, T. Thundat and H. Zeng, *ACS Appl. Mater. Interfaces*, 2019, **11**, 18720–18729.
27 G. Li, D. Chen, C. Li, W. Liu and H. Liu, *Adv. Sci.*, 2020, **7**, 2000154.
28 T. Li, L. Li, Y. Bai, Y. Cao, Q. Lu, Y. Li, G. Xu and T. Zhang, *Nanoscale*, 2019, **11**, 5737–5745.
29 C. Luo, J. Jiao, X. Su, L. Zheng, W. Yan and D. Zhong, *Nanomaterials*, 2022, **12**, 2325.
30 H. Niu, H. Zhang, W. Yue, S. Gao, H. Kan, C. Zhang, C. Zhang, J. Pang, Z. Lou, L. Wang, Y. Li, H. Liu and G. Shen, *Small*, 2021, **17**, 2100804.
31 G. Zhu, P. Ren, J. Wang, Q. Duan, F. Ren, W. Xia and D. Yan, *ACS Appl. Mater. Interfaces*, 2020, **12**, 19988–19999.
32 X. Wu, Y. Khan, J. Ting, J. Zhu, S. Ono, X. Zhang, S. Du, J. W. Evans, C. Lu and A. C. Arias, *Adv. Electron. Mater.*, 2020, **6**, 1901310.
33 S. R. A. Ruth, L. Beker, H. Tran, V. R. Feig, N. Matsuhisa and Z. Bao, *Adv. Funct. Mater.*, 2020, **30**, 1903100.
34 J. Qin, L. Yin, Y. Hao, S. Zhong, D. Zhang, K. Bi, Y. Zhang, Y. Zhao and Z. Dang, *Adv. Mater.*, 2021, **33**, 2008267.
35 L. Pan, A. Chortos, G. Yu, Y. Wang, S. Isaacson, R. Allen, Y. Shi, R. Dauskardt and Z. Bao, *Nat. Commun.*, 2014, **5**, 3002.
36 H. Joo, D. Jung, S. Sunwoo, J. Koo and D. Kim, *Small*, 2020, **16**, 1906270.
37 J. Zhou, H. Yan, C. Wang, H. Gong, Q. Nie and Y. Long, *Virtual Phys. Prototyp.*, 2022, **17**, 19–32.
38 J. Xie, L. Fan, D. Yao, F. Su, Z. Mu and Y. Zheng, *Mater. Today Chem.*, 2022, **23**, 100708.
39 K. Parida, G. Thangavel, G. Cai, X. Zhou, S. Park, J. Xiong and P. S. Lee, *Nat. Commun.*, 2019, **10**, 2158.
40 J. Kwon, Y. Lee, Y. Jo and S. Jung, *Org. Electron.*, 2018, **62**, 77–81.
41 C. Liu, C. Tsai, C. Chu, M. Chi, P. Chung and J. Chen, *Soft Matter*, 2018, **14**, 2772–2776.
42 W. Zhao, Z. Wang, J. Zhang, X. Wang, Y. Xu, N. Ding and Z. Peng, *Adv. Mater. Technol.*, 2021, **6**, 2001218.
43 X. Zhou, Y. Zhang, J. Yang, J. Li, S. Luo and D. Wei, *Nanomaterials*, 2019, **9**, 496.
44 N. Sakhuja, R. Kumar, P. Katare and N. Bhat, *ACS Sustainable Chem. Eng.*, 2022, **10**, 9697–9706.
45 P. Li, L. Zhao, Z. Jiang, M. Yu, Z. Li, X. Zhou and Y. Zhao, *Sci. Rep.*, 2019, **9**, 14457.
46 S. Kim, S. Mondal, B. Min and C. Choi, *ACS Appl. Mater. Interfaces*, 2018, **10**, 36377–36384.

47 W. Meng, X. Du, C. Ma and W. Li, *ACS Sustainable Chem. Eng.*, 2020, **8**(37), 14091–14100.
48 Y. Zhang, S. Liu, Y. Miao, H. Yang, X. Chen, X. Xiao, Z. Jiang, X. Chen, B. Nie and J. Liu, *ACS Appl. Mater. Interfaces*, 2020, **12**(25), 27961–27970.
49 A. R. Mohammadi, C. P. J. Bennington and M. Chiao, *J. Micromech. Microeng.*, 2011, **21**, 015009.
50 R. Ghosh, M. S. Song, J. B. Park, Y. Tchoe, P. Guha, W. Lee, Y. Lim, B. Kim, S.-W. Kim, M. Kim and G.-C. Yi, *Nano Energy*, 2021, **80**, 105537.